Thermal Runaway Characteristics and Failure Criticality of Massive Ternary Li-ion Battery Piles in Low-Pressure Storage and Transport

Yanhui Liu[a,b], Huichang Niu[c], Zhao Li[c], Jing Liu[d,*], Cangsu Xu[e], Xinyan Huang[a,b,*]

[a] *Research Centre for Fire Safety Engineering, The Hong Kong Polytechnic University, Hong Kong, China*

[b] *The Hong Kong Polytechnic University Shenzhen Research Institute, Shenzhen, China*

[c] *Guangzhou Institute of Industrial Technology, Guangzhou, China*

[d] *State Key Laboratory of Space Power Technology, Shanghai Institute of Space Power-Sources, Shanghai, China*

[e] *Department of Energy Engineering, Zhejiang University, Hangzhou, China*

* Corresponding to xy.huang@polyu.edu.hk (X. Huang); liujingbird86@163.com (J. Liu)

Abstract

Thermal runaway is a major safety concern for Lithium-ion batteries in manufacture, storage, and transport. Facing the frequent incidents in the air transport of massive batteries, more reliable fire prediction and protection strategies under low-pressures conditions are urgently needed. Herein, thermal runaway criticality of the open-circuit cylindrical battery piles (up to 9 cells with 30% SOC) under a hot boundary is investigated inside a novel low-pressure chamber (20-100 kPa). Characteristics battery temperatures for the safety venting and thermal runaway are measured to analyze the influences of pressure and cell number on battery failures. Results indicate that lowering the pressure could promote an earlier and stronger safety venting and weaken the intensity of the exothermic reactions inside cells, which is verified by the surface morphology of the electrodes. The overall fire risk is higher with higher pressure and larger battery-pile size, as indicated by the lower minimum boundary temperature for thermal runaway (255 °C~385 °C). Moreover, a simplified heat transfer model is established to explain the trend of thermal-runaway criteria and the influence of the low-pressure environment. This work delivers new insights into the effects of pressure and pile size on battery thermal runaway, which can help to improve the safe storage and transport of large-scale lithium-ion battery piles under varied pressure conditions.

Keywords: battery energy safety; open circuit; sub-atmospheric pressure; cell number; self-ignition

1. Introduction

Facing the crisis of fossil fuel depletion and environmental degradation, lithium-ion battery (LIB) is a promising energy-storage solution owing to high energy density, long lifespan, and limited pollution (Feng et al., 2020). To pursue a better electrochemical performance, active materials are applied in LIBs, inevitably causing the potential fire risk and hazards (Wang et al., 2019). Today, the LIBs are classified as Class 9 hazardous materials by the United Nations that have to pass the mandatory tests for their safe transport (United Nations, 2019). Nevertheless, the safety issue is still a significant obstacle to the large-scale storage and transport of LIBs. According to statistics from Federal Aviation Administration (FAA), more than 300 battery fires have been reported in air transport from January 2006 to June 2021 (Federal Aviation Administration, 2018), resulting in immense economic loss and safety concerns.

Thermal runaway is a common failure of battery, when the heat release rate from internal chain reactions larger than the external cooling rate. When thermal runaway occurs, LIBs rapidly release a large amount of heat and eject flammable and toxic materials (Sun et al., 2020). Once these flammable materials are ignited in the air, fire and explosion may occur (Cui and Liu, 2021). Safety engineering research has been done at the levels of component, cell, and module (or system) (Bravo Diaz et al., 2020; J. Sun et al., 2021). At the component level, stable electrode and flame-retardant electrolytes are developing to improve intrinsic battery safety. For a single cell, the underlying mechanism of internal heat generation (Bugryniec et al., 2019; Feng et al., 2019; Zhou et al., 2021), gas emission (Kennedy et al., 2021; Yuan et al., 2020), and external flaming combustion (Chen et al., 2020; Mao et al., 2020a; Ping et al., 2018) have been analyzed. At the module level, the synthetical influences of component chemistry (Said et al., 2020; H. Wang et al., 2020b), cell arrangements (Archibald et al., 2020; Huang et al., 2016), state of charge (SOC) (Lee et al., 2019; Li et al., 2019), and connection modes (Lamb et al., 2015; Lopez et al., 2015; Wang and Huang, 2020) on thermal-runaway propagation and suppression technologies (Torres-Castro et al., 2020; Weng et al., 2021, 2019; Yuan et al., 2021) are discussed.

During the storage and transport of massive open-circuit LIBs, although batteries are not in operation, many fire accidents still occur. To reduce the propensity of battery fire, FAA requires the SOC of cells lower than 30% in air transport (Federa Administration Aviation, 2016), and many shipping companies use refrigerated containers for battery transportation. Literature studies primarily focused on the effect of the ambient temperature, battery SOC and packing methods on thermal runaway characteristics. At standard atmospheric pressure, the possibility of self-heating ignition caused by poor heat dissipation within large-scale stored batteries has been experimentally investigated (He et al., 2020), theoretically derived (Y. Liu et al., 2020) and numerically verified (Hu et al., 2021b).

During the air transport, most freighter cabins have a sub-atmospheric pressure (e.g., 26 kPa at 10,000 m cruising altitude) to ensure fuselage structure stability, much lower than the 60-80 kPa in partially pressurized passenger airplanes (Fu et al., 2018; Q. Liu et al., 2020; H. Wang et al., 2020a). The effect of pressure is different on different aspects of fire risk. In general, lowering the pressure will reduce the environmental cooling that can make ignition easier, meanwhile, it can also weaken the flame to slow down burning and flame-spread processes (Huang and Gao, 2021; Nakamura et al., 2009; P. Sun et al., 2021). Therefore, the pressure effect on the onset and propagation of battery thermal-runaway processes can also be complex. Recent studies have looked into the battery thermal runaway behaviors and assess the fire hazards under low pressure (Chen et al., 2019b, 2019a, 2017; Fu et al., 2018; Q. Liu et al., 2020; H. Wang et al., 2020a; Xie et al., 2020a, 2020b, 2020c). The measured heat release rate of battery fire and the mass loss rate of cells showed the weaker battery fire and jet flame under lower pressure. However, influence of the pressure on the thermal-runaway criticality is more complex, especially the external heating sources (e.g., flame and radiant heater) that trigger the thermal runaway are also affected by the pressure. For example, Fu et al. (2018) found that reducing ambient pressure to 40 kPa can postpone the thermal runaway of a single cell. Nevertheless, a faster thermal runaway of LIB under low pressure was observed by Chen et al. (2017) and Xie et al. (2020a, 2020b). Moreover, most past low-pressure studies have not looked into LIBs of low-SOC (≤30%) and the safe pile size in storage and transport (Federa Administration Aviation, 2016). Therefore, there is a knowledge gap of the safety in low-pressure storage and

transportation of open-circuit LIBs.

In this work, the open-circuit cylindrical LIB piles with different pile sizes (or cell numbers) were tested under a hot boundary at ambient pressure ranging from 20 kPa to 100 kPa. Critical temperatures and chemical failure characterization for thermal runaway were quantified in terms of ambient pressure and cell number and analyzed by a simplified heat-transfer model. Results can advance the understanding of the pressure effect on battery thermal runaway and provide a scientific guideline for the safe storage and transport of massive LIBs.

2. Materials and Methods

2.1. Battery and apparatus

Cylindrical LIBs (ICR18650-22F) tested in this work were manufactured by Samsung SDI Co., Ltd, with a nominal capacity of 2.2 Ah and a nominal voltage of 3.6 V. The anode material of this LIB is made of intercalation graphite. The cathode material is the Lithium Nickel Manganese Cobalt Oxide ($LiNi_{0.5}Co_{0.2}Mn_{0.3}O_2$ or NCM 523): the element Ni is used to increase the energy density; element Co is employed to stabilize the laminate structure and enhance the cycling performance; the role of element Mn is cost reduction and safety promotion. The cell has a height of 65 mm, a diameter of 18 mm, and a mass of 41.05 ± 0.05 g. Before the experiment, a battery cycler (Neware, 5V/10A, ± 6 mA) was used to calibrate the SOC level of each cell to 30%, which is the maximum SOC value that FAA allowed for Li-ion batteries in air transport (Federa Administration Aviation, 2016). Specifically, each cell was fully charged to 4.2 V by Constant Current-Constant Voltage (CCCV) mode and then discharged with the constant current to 30% SOC. Afterward, all batteries were rested for 24 h to avoid the influence of internal heating during charging and discharging.
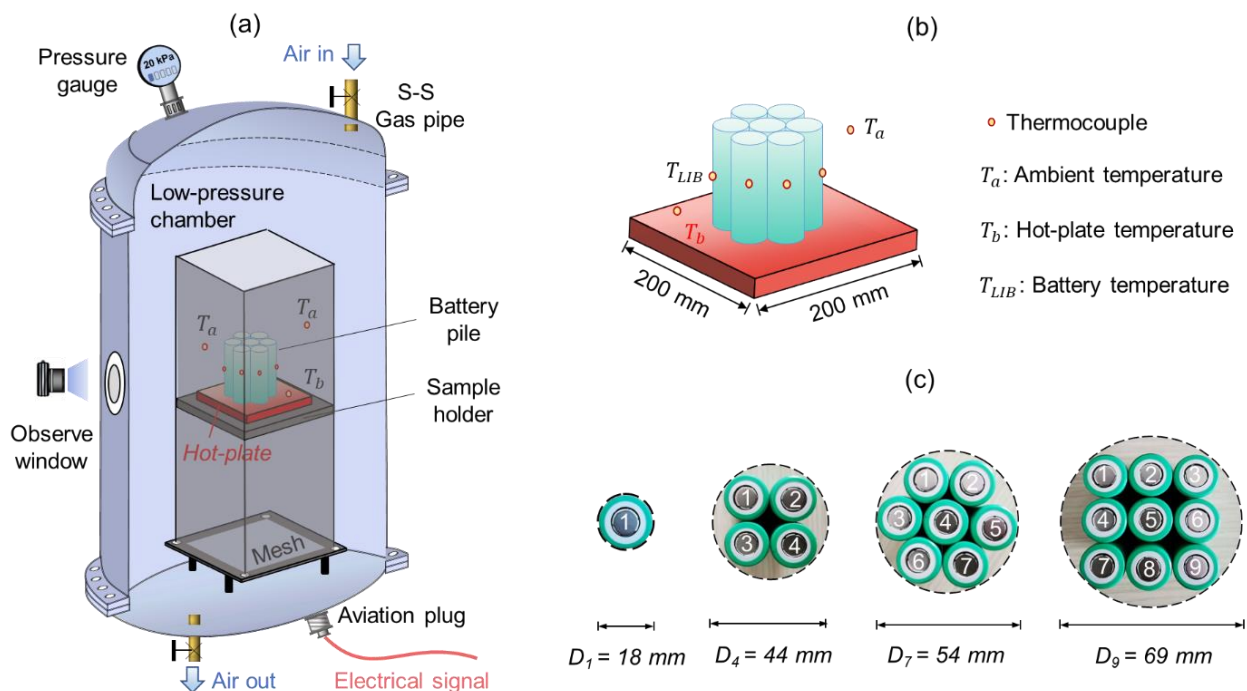

Fig. 1. Schematics of (a) low-pressure chamber, (b) hot-plate test, and (c) cylindrical battery piles.

A low-pressure chamber with an internal volume of 260 L was specially designed to provide a well-controlled environment (Fig. 1a). Compared with dynamic chambers in past studies, the sealed chamber

designed in this work is enclosed during the test to mimic the aviation transport condition. It can also achieve an ambient pressure from 0 kPa to 300 kPa, an ambient temperature from 20 °C to 60 °C, and an atmospheric with different gas composition. The chamber wall was made of the stainless-steel (SS) panel and coated with heat-insulating paint. A vacuum pump with an extraction rate of 600 L/min was attached to the chamber. By actively controlling the air inlet and air outlet, constant ambient pressure can be maintained, ranging from 0 kPa to 100 kPa in this work. Inside the pressure chamber, a cuboidal SS mesh was surrounding the testing battery cells to reduce the influence of inlet/outlet airflow and the impact of fire and explosion. During the experiment, the pressure gauge showed that thermal runaway of a single cell could lead to a pressure increase up to 0.8 kPa for a few seconds. Therefore, this chamber was large enough to limit the influence of venting gas on ambient pressure during the experiments.

To simulate the impact of external heating on the thermal runaway of the open-circuit LIB pile, the standard hot-plate test (ASTME 2021-01) was referred to (ASTM, 2014). Above the sample holder, a hot plate with a temperature accuracy of ± 1 °C was utilized to provide a hot boundary of the constant temperature up to 400 °C. As illustrated in Fig. 1b, the battery pile was placed on the center of the hot plate. Several K-type thermocouples with the bead diameter of 0.2 mm and an accuracy of 0.1 °C were used to measure the ambient temperature (T_a), battery temperature (T_{LIB}), and the hot plate temperature (T_b). The battery temperature (T_{LIB}) was employed as an indicator to capture the characteristic events during the tests. According to past experimental studies (Wang *et al.* 2020; Zhou *et al.* 2021), the axial temperature difference of LIB decreases with the SOC value during the vertical heating, so that the central surface temperature was adopted to characterize LIB temperature. Then, thin thermocouples were uniformly attached to the surface center of cells in all tests to monitor their temperatures (Fig. 1b). All temperature measurements were collected by a data logger, and a video camera was used to record the experiment inside the chamber through the observe window. Additionally, an electronic scale (±0.01 g) was employed to measure the mass of each battery cell before and after experiments.

2.2. Controlling parameters and testing methodology

In addition to the hot-boundary temperature, two key environmental and battery parameters are controlled in this work:

(1) *Ambient pressure.* Five pressures of 20 kPa, 40 kPa, 60 kPa, 80 kPa, and 100 kPa were selected. The high-power vacuum pump can help the chamber to reach the desired pressure quickly and accurately.

(2) *Number of cells (N) or size of the pile.* The battery piles of 1, 4, 7, 9 cells were tested where the open-circuit cells were horizontally stacked and fixed by thin stainless-steel (SS) wires to the cylindrical shape. Then, the equivalent diameter *(D)* of this cylindrical pile ranged from 18 mm (1 cell) to 69 mm (9 cells), as illustrated in Fig. 1c and Table 1.

Table 1. Characteristics of cylindrical battery piles.

No. of Cells (-)	1	4	7	9
Pile diameter, D (mm)	18	44	54	69
Pile height, H (mm)	65	65	65	65

Before the test, the hot plate was first preheated to the target boundary temperature (T_b), ranging from 200 °C to 400 °C. Once the targeted temperature was reached, it would be stabilized for at least 10 min. Then, the prepared battery pile was carefully placed in the center of the hot plate, ensuring good contact between the bottom surface (negative) of the battery pile and the top surface of the hot plate. Then, the pressure chamber was airtight, and the vacuum pump turned on until the ambient pressure decreased to the desired value. As the rated extraction speed of the vacuum pump is about 600 L/min, it takes less than 2 min for the chamber to reach the target pressure.

Referring to the Standard Test Method for Hot-Surface Ignition ASTME 2021 (ASTM, 2014) and studies related to LIB thermal runaway (Börger et al., 2019; Feng et al., 2019), two criteria were utilized in this work to determine the occurrence of thermal runaway. Specifically, (i) the surface temperature of LIB is at least 50 °C above the hot boundary temperature, and (ii) the temperature rise rate of the LIB is higher than 1 °C/s. When both criteria are satisfied, the LIB is considered to reach the thermal runaway.

Determining critical boundary temperature to trigger thermal runaway followed the procedures in our previous work with pouch batteries (Liu et al., 2021). Two characteristic boundary temperatures were employed in this work. The *supercritical temperature* was regarded as the minimum hot boundary temperature that thermal runaway required. The *subcritical temperature* was defined as the maximum hot boundary temperature that can prevent thermal runaway. The timeframe for determining these two characteristic temperatures is 2 h (i.e., observing the LIB piles for thermal runaway during the two-hour heating time). After heating tests, cells without thermal runaway would be placed in a fireproof chamber and observed for at least 5 h under a constant temperature of 25 °C. Experiments were conducted using different hot-boundary temperatures until the temperature difference between the supercritical and subcritical ignition temperature was less than 10 °C. Then, the critical boundary temperature (T_b^*) for thermal runaway is the average value of these two temperatures. All tests near the critical conditions were repeated at least three times to reduce the experimental errors.

2.3. Surface morphology of the electrodes after tests

After thermal-runaway tests, all burnt cells were collected and placed in a drying chamber with a constant temperature of 25 °C for 5 h. Then, these cells were disassembled in a glove box. Scanning electron microscopy (SEM) - Energy dispersive spectrometer (EDS) analysis was conducted to characterize the morphology and composition of electrodes. A ZEISS Gemini Sigma 300 field emission SEM coupled with EDS (Oxford Aztec X-Max20) was employed in this work.

3. Results

3.1. Thermal behavior of battery pile

Fig. 2 demonstrates the typical processes for a successful and a failed thermal runaway of the 4-cell battery piles at 100 kPa. As shown in Fig. 2a, thermal runaway did not occur when the hot-plate temperature (T_b) was 265 °C. For this case, the battery pile was heated by the hot plate in the first 18 min. During the heating, the positive caps slightly bulged, indicating the exothermic reaction initiation and gas generation inside cells. As exothermic reactions proceeded, more and more gases were generated and increased the internal pressure of cells. At around 19 min, the safety valve of cell-2 firstly broke since it cannot withstand high internal pressure.

This bursting behavior of cells successively happened within three minutes, along with the ejection of little gas and some insulator materials near the positive cap. After the gas releasing stage, all cells reached the thermal equilibrium, and no thermal runaway was observed after 1 h.

For the case of successful thermal runaway in Fig. 2b, the hot-plate temperature (T_b) was constant at 275 °C. The slight bulging of positive caps was also observed during the heating stage. However, the safety venting was earlier, and the gas release was much more intense. Finally, a large amount of smoke was released in a short period, indicating the occurrence of thermal runaway. Unlike fully charged cells, the thermal runaway of cells with 30% SOC did not trigger violent combustion, which was consistent with the phenomenon observed previously (Liu et al., 2020) and in many studies (Fu et al., 2015). The mass loss for the burnt cell is 5 g (i.e., around 12% of the original mass). Therefore, 30% SOC is relatively safer for batteries in storage and transport. However, the thermal runaway of 30% SOC cells and the release of flammable and toxic emissions still can intensify the fire event and pose a significant threat to public safety.
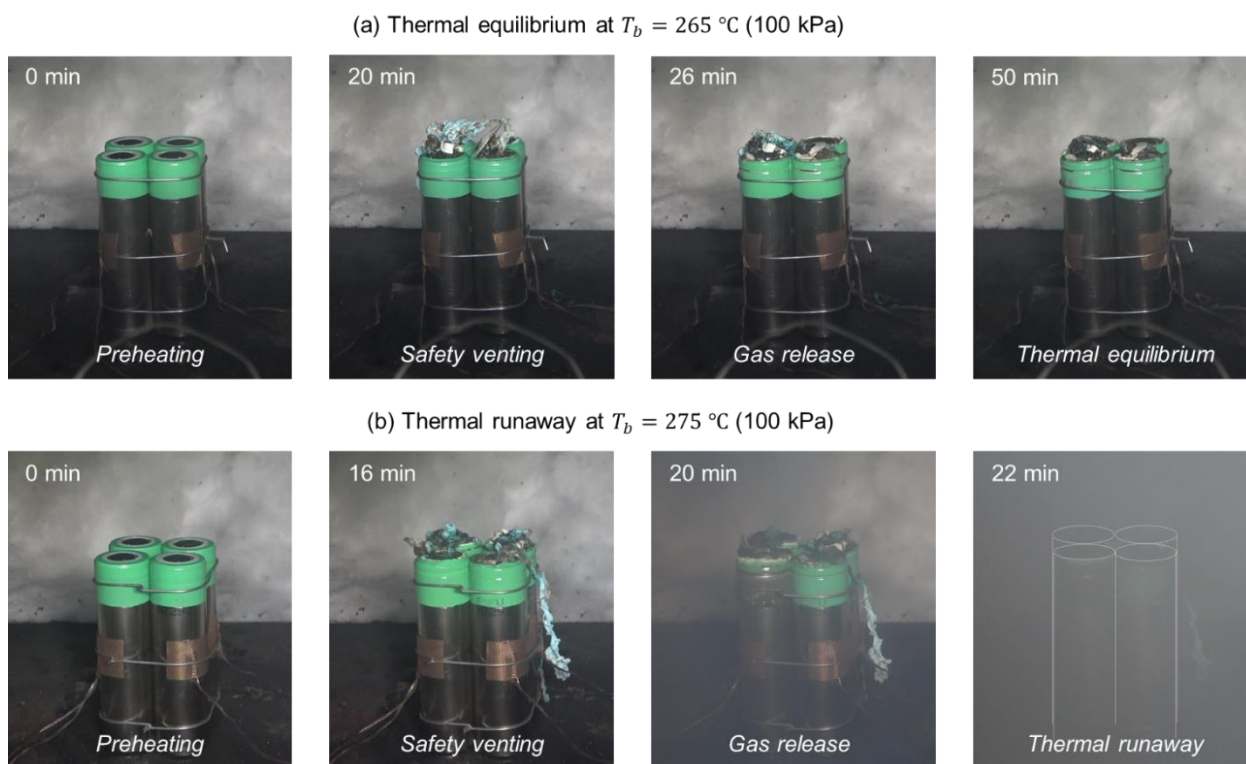

Fig. 2. Experimental phenomena of the 4-cell battery pile at 100 kPa, (a) thermal equilibrium at the boundary temperature of 265 °C (Video S1), and (b) thermal runaway at the boundary temperature of 275 °C (Video S2).

To better analyze the thermal behaviors of battery piles under the hot boundary, temperature evolution curves corresponding to two tests in Fig. 2 are presented in Fig. 3. For the thermal-equilibrium case (Fig. 3a), the battery pile underwent three stages: (I) preheating, (II) venting, and (III) thermal equilibrium. Initially, the surface temperatures of the cells escalate with an average rate of 0.2 °C/s due to the hot-plate heating. During the preheating stage, a sudden temperature increasing from 121 °C to 146 °C of cell-4 can be observed (purple line). This phenomenon is attributed to the micro short circuit (MSC) inside the cell, which is related to the separator defects (Li et al., 2019). At around 19 min, a minor fluctuation appears at the temperature curve of cell-2 (black line), which suggests the appearance of the safety valve bursting. Then, gases and heat inside the

cells can be emitted to the environment through the holes of failed safety valve. However, this temporary cooling is not enough to suppress the self-heating reactions inside the battery. The chemical materials continue to react until running out. Finally, this battery pile reaches thermal equilibrium.
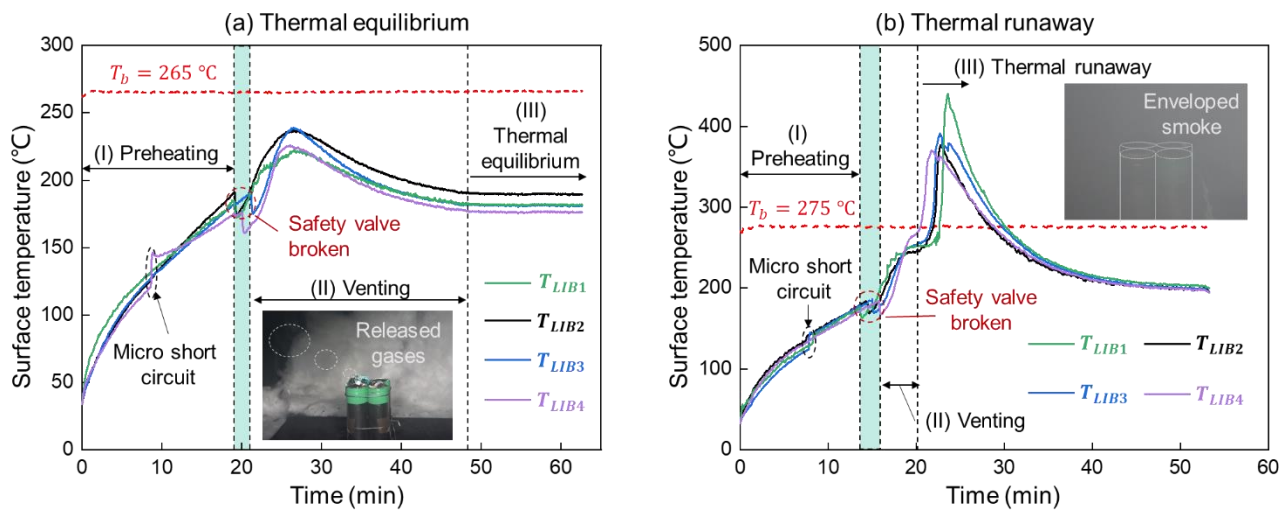

Fig. 3. Temperature variations of the 4-cell battery pile at 100 kPa, (a) no thermal runaway at $T_b = 265\,°C$, and (b) thermal runaway at $T_b = 275\,°C$.

In terms of the thermal-runaway case, temperature variation curves are depicted in Fig. 3b. Similarly, the thermal runaway process can be divided into three stages: (I) preheating, (II) venting, and (III) thermal runaway. During the preheating stage, the cell temperatures increase steadily under continuous heating by the hot plate. A slight temperature increase induced by MSC can be seen when the cell temperature reaches about 125 °C. This MSC temperature is close to the melting point of the separator material used in this work (polyethylene), further confirming that the occurrence of MSC is separator flaws related. At 14 min, the safety valve of cell-1 broke, and the failure of the other safety valves happened within two minutes. During the venting stage, the cell temperatures keep rising with an average rate of 0.35 °C/s. Finally, thermal runaway occurs, which is marked by the sharp temperature increase of the cells and a tremendous amount of smoke releasing.

3.2. Safety venting and thermal runaway

To further explore the pressure effect on thermal runaway behavior, Fig. 4 shows the temperature evolution curves of 4-cell piles at the boundary temperature of 330 °C under different ambient pressures. Apparently, temperature evolution curves exhibit a similar trend for the thermal runaway cases where two crucial moments of safety venting and thermal runaway divide the experimental process into three phases. Therefore, four key parameters of safety venting temperature T_v, thermal runaway onset temperature T_{TR}, maximum surface temperature after thermal runaway T_{max}, and the time interval (or the delay) from safety venting to thermal runaway Δt are employed in this section to study the pressure influence on the thermal runaway (Fig. 4).

As mentioned before, safety valve bursting is a transition point from preheating to venting during the thermal runaway process. The previous studies found that safety venting temperature (T_v) is closely related to the cathode materials and SOC level of battery cells (Liu et al., 2015). As shown in the orange bar graph in Fig. 4d, T_v for 30% battery piles at 20 kPa, 60 kPa, and 100 kPa are 187±4 °C, 179±5 °C, and 185±1 °C, which is insensitive to the ambient pressure.

Thermal runaway onset temperature (T_{TR}) and maximum surface temperature after thermal runaway (T_{max}) are two important parameters to evaluate the thermal stability and thermal hazards of batteries. Increasing T_{TR} or decreasing T_{max} could be the basic principle for the safety design of the battery pack. As shown in the green bar graph in Fig. 4d, T_{TR} for 30% battery piles at 20 kPa, 60 kPa, and 100 kPa are 306 ± 3 °C, 291 ± 5 °C, and 278 ± 6 °C, respectively. For 30% battery piles at 20 kPa, 60 kPa, and 100 kPa, T_{max} are 420 ± 9 °C, 450 ± 22 °C, and 455 ± 15 °C, respectively (purple bar graph in Fig. 4d). Therefore, with the pressure decreasing, T_{TR} shows an increasing trend while T_{max} performs a declining trend, indicating a lower thermal runaway risk.
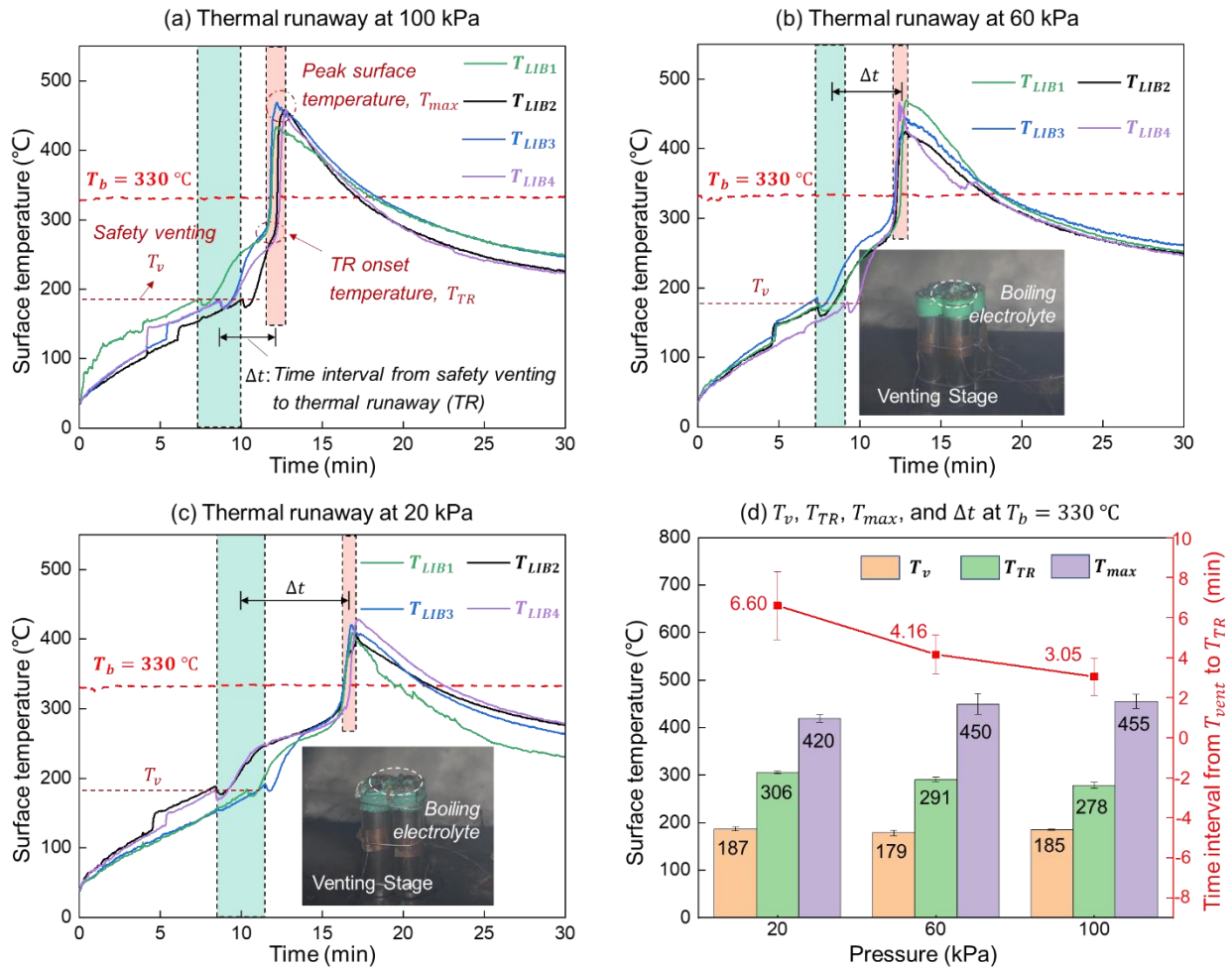

Fig. 4. The temperature evolution curves of the 4-cell battery pile at the hot plate of 330 °C under the ambient pressure of (a) 100 kPa, (b) 60 kPa, and (c) 20 kPa; as well as (d) the safety venting temperature T_v, thermal runaway temperature T_{TR}, maximum surface temperature T_{max}, and the time delay from T_v to T_{TR}.

Since the safety venting temperature is insensitive to the ambient pressure, whereas the thermal runaway onset temperature increases with the decreasing pressure, the pressure has a significant influence on the venting stage. Such influence can be observed during the experiments. Specifically, the boiling of electrolytes is more visible at 60 kPa and 20 kPa (see Videos S3 and S4). It can be deduced that evaporation and volatilization of electrolytes were accelerated under low pressure. Additionally, Fig. 4d compares the time delays from safety venting to thermal runaway (Δt) under these three pressure levels, where Δt increases from 3.05 min to 6.60 min as the ambient pressure decreases from 100 kPa to 20 kPa. The delay of thermal runaway results from the

lower heat accumulation rate under lower pressure. Therefore, low pressure can weaken the intensity of exothermic reactions by accelerating the evaporation and volatilization of electrolytes.

To comprehensively analyze the effects of ambient pressure and cell number on thermal runaway characteristics, Fig. 5 summarizes the T_v, T_{TR}, T_{max}, and Δt of battery piles at all supercritical conditions. As expected, safety venting temperature T_v (around 186.91 ± 15.09 °C) is less sensitive to ambient pressure. The latest research findings suggest that the pressure inside a cylindrical cell can exceed 1.2 MPa before safety venting (Qin et al., 2021), which is much higher than the pressure gradient (0.02 MPa) in this work. Therefore, the safety venting temperature is mainly related to the internal electrochemical reactions.
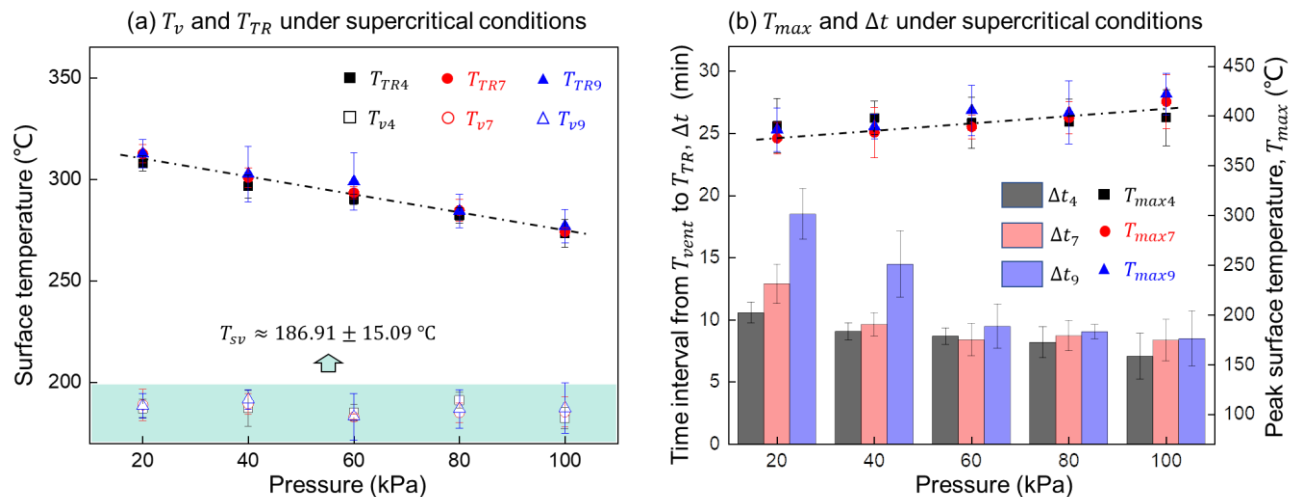

Fig. 5. The characteristic temperatures and times of the battery piles with different pile sizes and ambient pressure at the supercritical conditions for thermal runaway: (a) T_v and T_{TR}, and (b) T_{max} and Δt (numbers of " 4, 7, and 9" represent the cell number of the battery pile).

Furthermore, the thermal runaway onset temperature (T_{TR}) increases with decreasing ambient pressure (Fig. 5a). This is because the evaporation and volatilization of electrolyte and flammable gases will be enhanced after the safety valve rupture, resulting in fewer reactants of self-heating reactions and lower heat accumulation under low pressure (see more discussion in Section 4.2). Due to the relatively weak electrochemical reactions, the maximum battery temperature after thermal runaway (T_{max}) slightly decreases with ambient pressure.

Different from those characteristic temperatures, which are irrelevant to cell number (or battery pile size), the time delay from safety venting to thermal runaway (Δt) is significantly affected by both ambient pressure and cell number. As shown in the bar chart of Fig. 5b, Δt lengthens as ambient pressure decreases or cell number increases. It is because the exothermic reaction is less intense at a low pressure, which needs more time to provide energy for thermal runaway. For larger battery piles, reaching the battery's minimum thermal runaway energy is postponed due to the large fuel loads. In the real scenario, such a time delay can be regarded as the effective fire prevention time. Therefore, a lower pressure can provide a longer emergency response time to prevent the thermal runaway propagation and fire event in the battery pile.

3.3. Chemical analysis of electrodes

To further verify the pressure effect on the exothermic reactions after safety venting, SEM/EDS analysis

was conducted to characterize the chemical failure of the electrodes under different pressure. This method is extensively adopted in studies to investigate the failure characteristics of LIBs (Huang et al., 2020; H. Wang et al., 2020b). Fig. 6a shows the SEM/EDS results of the electrode materials for fresh cells under 1k magnification.
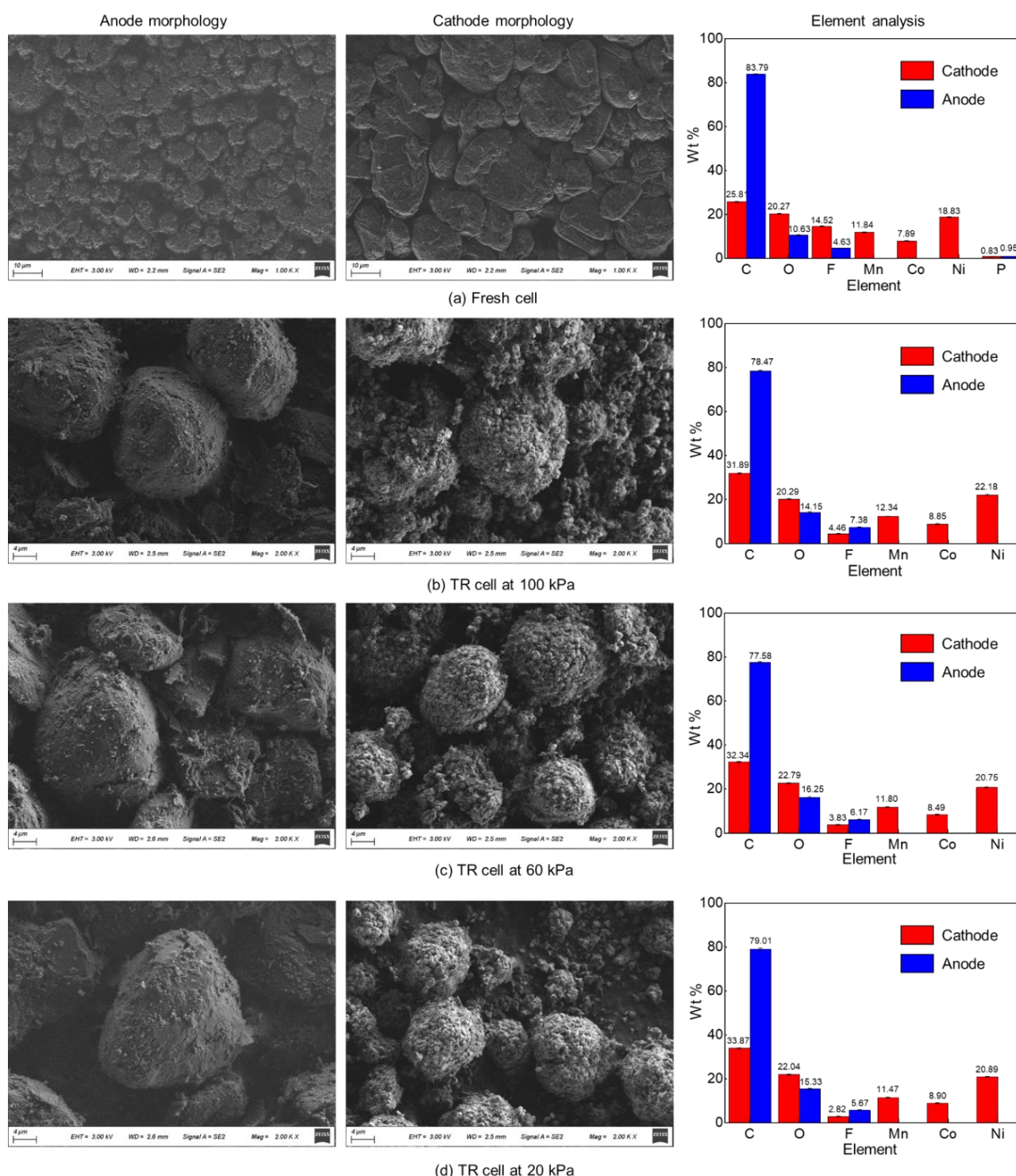

Fig. 6. SEM/EDS results for the electrodes of the (a) fresh cell, (b) thermal runaway cell at 100 kPa, (c) thermal runaway cell at 60 kPa, and (d) thermal runaway cell at 20 kPa.

Before the experiments, the surfaces of both anode and cathode material are relatively flat and tidy. It is found that the major elements for fresh cathode are carbon (C), oxygen (O), fluorine (F), manganese (Mn), cobalt (Co), nickel (Ni), and phosphorus (P) with contents of 25.81%, 20.27%, 14.82%, 11.84%, 7.89%, 18.83%,

and 0.83%, respectively. For the fresh anode material, the significant elements of C, O, F, and P account for 83.79%, 10.63%, 4.83%, and 0.95%, respectively. In order to detailly characterize the different surface morphology after the thermal runaway, Fig. 6b-d exhibit the SEM/EDS results of the electrode materials for burnt cells under 2k magnification. Apparently, the deformation of the cathode material is server than that of the anode, and more caves and holes exist on the cathode surface. The corresponding reason is that the disproportionation and decomposition of the cathode material contribute to the major heat during thermal runaway, and the gases primarily release from the cathode.

In terms of EDS results for cathode materials after the thermal runaway, the decrease of element F is significant, which is caused by the consumption of the electrolyte and binder during the thermal runaway process. For example, the content of element F decreases from 14.52% to 4.46% after thermal runaway at 100 kPa. In addition, the content of F in the cathode residue decreases with the ambient pressure. For cathode residues of cells at 100 kPa, 60 kPa, and 20 kPa, F accounts 4.46%, 3.83%, and 2.82%, respectively. At standard atmospheric pressure, lower F contents in cathode residue mean higher electrolyte consumption during thermal runaway, indicating a higher degree of exothermic reaction inside the battery. At lower pressure, although the content of element F is lower, the intensity of the exothermic reaction is relatively weak (Fig. 5). It confirmed that the electrolyte loss is mainly caused by evaporation and volatilization rather than reaction consumption under low pressure.

These results are also consistent with the findings presented by researchers from the National Aeronautics and Space Administration (NASA), where the particulates generated by LIB thermal runaway in vacuum conditions were collected and analyzed (Nemanick et al., 2018). Based on chemical analyses such as SEM/EDX (energy dispersive X-ray), Fourier-transform infrared spectroscopy (FTIR), and Gas chromatography–mass spectrometry (GC-MS), it is found that the volatile electrolyte components performed a higher percentage in particulate compositions. For EDS results of anode materials after thermal runaway, the variation of element C is more significant than element F. This is due to the high consumption of C in the reaction between anode and electrolyte, and the decrease in C corresponds to the increase in O and F. Therefore, the weak thermal runaway intensity is attributed to the strong volatilization of the electrolyte after safety venting under low pressure.

3.4. Critical boundary temperature

Fig. 7 summarizes the critical boundary temperature to trigger thermal runaway (T_b^*) varying with the ambient pressure and cell number (or pile size), where the error bar shows the variation from the repeating tests. It is evident that the value of T_b^* decreases with the ambient pressure. Specifically, the critical boundary temperature for the thermal runaway of the 9-cell battery pile decreases from 280 °C to 255 °C, as the ambient pressure increases from 20 kPa to 100 kPa. For the 4-cell battery piles, the critical boundary temperature decreases from 305 °C (20 kPa) to 270 °C (100 kPa) with a decrement of 11.5%.

For the 1-cell battery piles, the value of T_b^* is 345 °C at 100 kPa, whereas it is higher than 400 °C at 40 kPa. Since the maximum temperature of the hot plate is 400 °C, the critical boundary temperatures for thermal runaway of the single cell at and below 40 kPa are not quantified. To trigger the thermal runaway of a single cell, a much hotter boundary is needed, that is, 70-100 °C higher than that for battery pile. This result also suggests that it is inappropriate to just test the single battery cell and using its results to do safety design of large

battery piles, which will significantly underestimate the risk of thermal runaway and fire events.
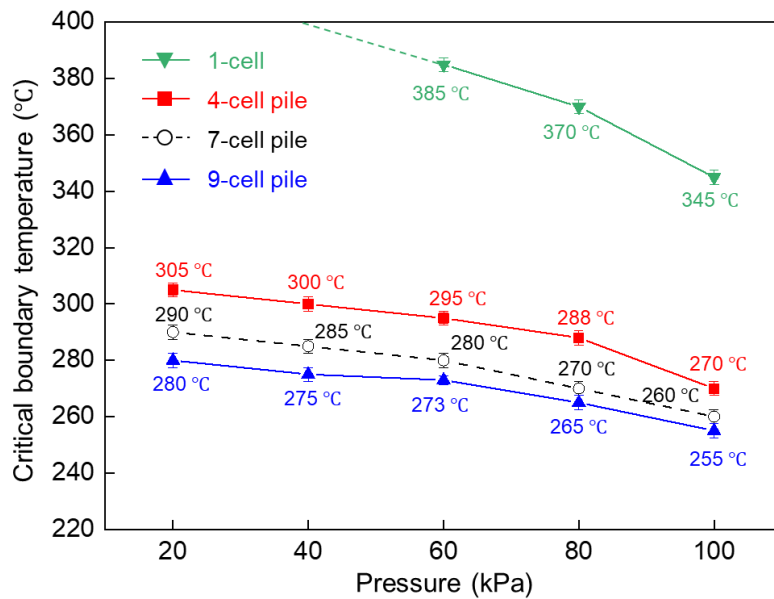

Fig. 7. The critical boundary temperature (T_b^*) varying with ambient pressure and cell number.

Moreover, the value of T_b^* also decreases with the cell number. For example, when the ambient pressure is 20 kPa which could be the minimum pressure level in air transport, T_b^* decreases from 305 °C to 280 °C as the pile increases from 4 cells to 9 cells. Therefore, the critical boundary temperature decreases with both ambient pressure and cell number. In other words, battery piles with a larger size and higher ambient pressure have a higher risk of thermal runaway and fire.

4. Discussions

4.1. Environmental cooling under low pressure

The cooling condition plays a crucial role in battery thermal management, which can benefit the working performance and lifecycle of batteries (Offer et al., 2020). For the open-circuit battery piles in storage and transport, the environmental cooling coefficient controls the thermal runaway risk (Hu et al., 2020). At the subcritical equilibrium state (e.g., Fig. 3a), the exothermic reaction inside the cell is negligible, and the temperature differences between cells are much lower than temperature differences between cells and hot plate. Specifically, in Fig. 3a, the average temperature difference between cells is about 5.7 °C, while the average temperature between cells and hot plate is 83 °C. Therefore, the heat transfer between cells is much lower than that between LIB pile and hot plate, and the external heating ($\dot{q}_{ex}$) from the hot plate should balance with the environmental cooling ($\dot{q}_{loss}$) from other surfaces (Fig. 8a) as

$$\dot{q}_{ex} = A_p k_{LIB} \frac{T_b - T_{LIB}}{H/2} = \dot{q}_{loss} = A_{pc} h(T_{LIB} - T_a) \tag{1}$$

where A_p is the bottom area of the battery pile; A_{pc} is the cooling surface area of the battery pile; T_b is the temperature of hot boundary; T_{LIB} is the average temperature of cells; $T_a = 300$ K is ambient temperature; and k_{LIB} is thermal conductivity of the battery cell in axial direction which can be regarded as 30.4 W/m-K for a ternary 18650 cell (Drake et al., 2014).

The overall cooling coefficient (h) includes both convection (h_c) and radiation (h_{rad}) as

$$h = \frac{2A_p k_{LIB}(T_b - T_{LIB})}{A_{pc} H (T_{LIB} - T_a)} = h_c + h_{rad} \tag{2}$$

The radiative cooling coefficient can be estimated as

$$h_{rad} = \varepsilon \sigma (T_{LIB}^2 + T_a^2)(T_{LIB} + T_a) \tag{3}$$

where $\sigma = 5.67 \times 10^{-8}$ W/m^{2}K^4 is the Stefan–Boltzmann constant; and $\varepsilon \approx 0.9$ is the effective surface emissivity. The convective cooling coefficient (h_c) is

$$h_c = h - h_{rad} = Nu \frac{k_a}{L} \propto Gr^m \propto \rho^{2m} \propto P^{2m} \quad (m > 0) \tag{4}$$

where Nu is the Nusselt number; Gr is the Grashof number; k_a is the conductivity of air; and L is characteristic length, respectively; ρ is the air density. Therefore, as the pressure decreases, the convective coefficient h_c and environmental cooling decreases.
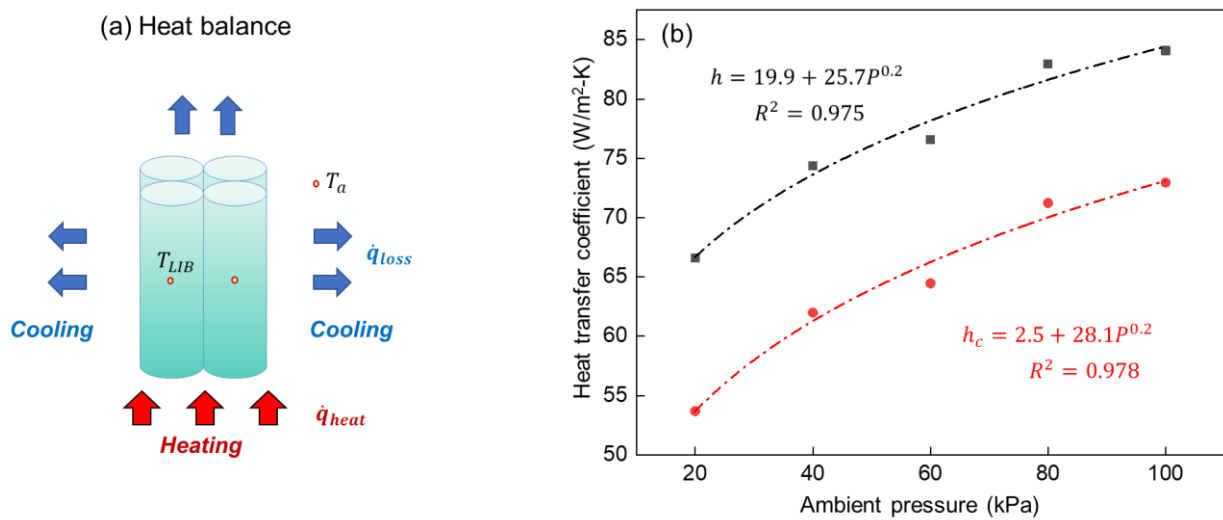

Fig. 8 (a) Schematic diagram of heat transfer condition at thermal equilibrium stage and (b) relationship between ambient pressure and calculated overall cooling coefficient h, as well as convective coefficient h_c.

Table 2. The calculated effective cooling coefficient $h = h_c + h_{rad}$ of the 4-cells pile.

| P | T_b | T_{LIB} | h | h_{rad} | h_c |
(kPa)	(K)	(K)	(W/m²-K)	(W/m²-K)	(W/m²-K)
100	541	449	84.1	11.1	73.0
80	558	460	82.9	11.7	71.2
60	563	468	76.6	12.1	64.5
40	568	473	74.4	12.4	62.0
20	573	483	66.6	12.9	53.7

Inputting the experimental data under different pressures and cell numbers, all cooling coefficients (h, h_c, and h_{rad}) can be calculated from Eqs. (2-4). Using the 4-cell piles ($A_p = 1.52 \times 10^{-3}$ m^2, $A_{pc} = 1.05 \times 10^{-2}$ m^2, H = 0.065 m) as an example, the key parameters at the thermal equilibrium state are calculated and summarized

in Table 2 and Fig. 8b. First of all, the value of h decreases with the decreasing ambient pressure, showing a weak cooling condition under low ambient pressure. Moreover, the convective cooling ($h_c \propto P^{0.2}$) plays the major role, which is 5 times greater than the radiative cooling.

4.2. Effect of pressure on venting

As discussed above, environmental cooling decreases by lowering the environmental pressure, which may accelerate the thermal runaway of the battery pile, indicating a higher fire risk. However, thermal runaway temperature and fire risk of battery pile are lower in a lower pressure in Fig. 7, presenting an opposite trend. Considering the safety vent opens at a critical pressure difference between internal and ambient ($\Delta P^* = P_{in} - P$), under lower ambient pressure (P), the venting will occur earlier at a lower internal pressure (P_{in}).

After the bursting of the safety valve, more internal electrolytes and other active materials are evaporated and volatilized. Under a larger pressure difference, these materials are escaped at a faster rate as

$$\dot{m}_e = \rho_e V_e \sim \Delta P = P_{in} - P \tag{5}$$

The ventilation velocity (V_e) increases with pressure difference by following either Darcy's law (infiltration) or Bernoulli's law (discharged flow) as

$$V_e = \begin{cases} \dfrac{k_d A}{\mu} \dfrac{\Delta P}{\Delta x} \propto \Delta P & \text{[Darcy's law]} \\ \sqrt{2\rho_e \Delta P} \propto \sqrt{\Delta P} & \text{[Bernoulli's law]} \end{cases} \tag{6}$$

where k_d is permeability (m^2); and μ is dynamic viscosity (Pa-s). Faster and stronger evaporation under a lower pressure was also observed in the experiments (see Videos S3 and S4). Therefore, the reactants inside the battery and exothermic reactions drop at lower pressure, resulting in a lower internal heat release rate.

4.3. Thermal-Runaway Criticality

When the critical condition of thermal runaway ($T_{LIB} = T_{TR}$), the battery internal exothermic reactions become important. Given that the temperature difference within the LIB pile is still much lower than the temperature difference between LIB and hot boundary, two primary heating mechanisms are considered in the heat transfer model, that is, external heating caused by the hot boundary ($\dot{q}_{ex}$) and internal heating caused by exothermic reactions ($\dot{q}_r$). Thus, the critical thermal balance equation can be expressed as

$$\dot{q}_{ex} + \dot{q}_r = \dot{q}_{loss} \tag{7}$$

Recent studies suggest that the overall exothermic reaction can be simplified as a one-step Arrhenius equation when the LIB approach to TR condition (Mao et al., 2020b; Qin et al., 2021; J. Sun et al., 2021) and increases with the battery internal pressure (Fu et al., 2018) as

$$\dot{q}_r = m_{LIB} Z \exp\left(-\frac{E}{RT_{TR}}\right) \Delta H \propto P_{in}^n = (\Delta P^* + P)^n \tag{8}$$

where Z is the pre-exponential factor; E is activation energy; ΔH is heat of reactions; m_{LIB} is the mass of battery pile; and $n = 4.3$ was found in the experiment conducted by Fu et al. (Fu et al., 2018). From Eq. (1), we have

$$\frac{2A_p k_{LIB}}{H}(T_b^* - T_{TR}) + \dot{q}_r = A_{pc} h(T_{TR} - T_a) \tag{9}$$

With the cooling coefficients calculated from Eqs. (2-4), the critical boundary temperature for thermal runaway (T_b^*) can be expressed as

$$T_b^* = T_{TR} + \frac{H}{2A_p k_{LIB}}\left[A_{pc}h(T_{TR} - T_a) - \dot{q}_r\right] \propto \frac{1}{D} \tag{10}$$

where the battery pile cross-section area ($A_p = \pi D^2/4$), cooling surface area ($A_{pc} \approx \pi DH + \pi D^2/4$), and high ($H$) depends on the size and shape of the pile, while k_{LIB} and T_{TR} are fixed for the given LIB type and SOC.

Therefore, T_b^* decreases with the equivalent diameter (or size) of battery pile (D), agreeing the lower critical boundary temperature for a bigger battery pile with more cells (see Fig. 7). On the other hand, as the pressure decreases, although the convective cooling slightly decreases ($h \propto P^{0.2}$), the reduction of the self-heating inside the vented battery is more significant ($\dot{q}_r \propto P^{4.3}$). Thus, the critical boundary temperature for a thermal runaway is higher under lower ambient pressure (Fig. 7), showing a lower overall fire risk. Therefore, Eq. (10) can successfully demonstrate the influences of ambient pressure and cell number on the critical boundary temperature for thermal runaway.

For the 1-layer battery pile with an infinite diameter ($H = 65\ mm, D \rightarrow \infty$), T_b^* will eventually drop to a constant value, which is consistent with the theoretical prediction results for the self-ignition of large-scale battery pile in our previous work (Y. Liu et al., 2020). Except for the ambient pressure and pile size, this critical boundary temperature (T_b^*) is also affected by several factors, such as ambient temperature, SOC level, and LIB chemistry. In future, the synthetic effect of these factors will be numerically analyzed. And an accurate model to predict the critical boundary temperatures (vs pressure or other factors) of high-energy batteries will be proposed with the aid of chemical kinetic data from the accelerating rate calorimetry (ARC) tests.

4.4. Implications and Applications

Although the effect of environmental cooling on battery pile is relatively weaker at a lower pressure, it is more difficult to trigger the thermal runaway by external heating. It is because, at a lower pressure, the safety valve opens earlier at a lower battery temperature. Due to the larger pressure difference, more active materials are escaped, leading to the weaker exothermic reactions inside the battery so does the later thermal runaway. This phenomenon is counter-intuitive and has several important implications in the battery safety application.

Influence of the environment. When the environmental conditions like pressure, oxygen level and humidity change, they may have different impacts on the different safety aspects of the battery and different stages of battery fire. For example, reducing the pressure can (1) reduce the environmental cooling, (2) cause an early venting, and (3) reduce the flame intensity. Thus, the overall effect of pressure is complex, and it is difficult to simply judge that reducing the ambient pressure can increase/decrease the battery thermal safety or conclude that the low-pressure air transport of battery pile is more/less dangerous.

Number of cells vs. safety. Compared to a single battery, the thermal runaway becomes much easier even for a smaller pile with a number of battery cells. The risk of failure and fire further increases, as the number and size increases, and the thermal runaway can occur under a lower external thermal impact. Similar trends have also been observed in the hot oven tests and verified by the numerical simulations (He et al., 2021; Hu et al., 2021a). Therefore, except for limiting the maximum value of battery SOC, it is also important to regulate the maximum number of cells in the storage and transport and add barriers to divide large piles into smaller groups.

Fire protection strategies for battery energy storage systems. Experimental results indicate that the time interval between safety venting and thermal runaway will increase with decreasing pressure. Thus, the depressurization or ventilation system could be an effective fire protection approach to ensure the safety of energy storage systems with massive LIBs. For example, once the venting signal is detected by the battery management system, reducing the ambient pressure to a low value can not only mitigate the risk of thermal runaway, but also provide sufficient time to diagnose faults and take emergency measures.

Threshold design of safety valve. Safety valve is an important configuration to prevent the cell from explosion. The battery pile exhibits a lower thermal-runaway risk at lower pressure owing to an earlier venting the higher volatilization rate of electrolyte. However, the threshold design of the safety valve has not been clearly defined. Since several studies suggested that the internal pressure can exceed 1.2 MPa before thermal runaway, threshold ranging from 1.3 MPa to 1.6 MPa has been widely selected by the manufacture for safety valve. Nowadays, the energy density of battery gradually increases, indicating the higher gas generation rate under unusual conditions. If the threshold of safety valve is too high, the probability of explosion will be greatly increased. If the threshold of safety valve is too low, the recycling capacity and state of health will be influenced. In airplanes and spacecraft, many high-energy-density batteries operate at sub-atmospheric pressure. Therefore, the threshold pressure of safety valve of cells in these low-pressure applications may be set lower than standard values to achieve better safety features.

5. Conclusions

In this work, the thermal-runaway behaviors of 30% SOC LIB piles at the ambient pressure ranging from 20 kPa to 100 kPa were investigated in a novel low-pressure chamber. The battery failure process was separated by two important moments of safety venting and thermal runaway. Lowering the pressure could lead to an earlier safety venting and postpone the thermal runaway. The safety venting temperature (187 °C) was irrelevant to both ambient pressure and cell number, whereas the thermal-runaway temperature (270~310 °C) increased with decreasing pressure. During the venting stage, active materials inside the battery were more prone to escape under low pressure, resulting in a weak exothermic reaction and a slow heat accumulation. Such a phenomenon was further verified by the SEM/EDS analysis of the burnt cathodes, where a dramatic reduction in element F can be observed under the sub-atmospheric pressure.

As the pressure decreased, the minimum boundary temperature for thermal runaway increased, indicating a lower overall fire risk. As the number of cells increases, the thermal runaway occurred at lower external heating, indicating a higher fire risk. Moreover, a simplified heat transfer model was proposed to demonstrate the effects of pressure and battery pile size on thermal-runaway criteria. In this way, the mechanism of pressure effect on thermal runaway is revealed, which is a significant addition to the literature and helps to improve the fire safety of battery piles during storage and transport.

Nomenclature

Symbols

A	surface area (m^2)
D	battery pile diameter (m)
E	activation energy (J/mol)
Gr	Grashof number (-)
h	heat transfer coefficient (W/m^2-K)
H	battery height (m)
ΔH	heat of reactions (kJ/kg)
k	thermal conductivity (W/m-K)
L	characteristic length (m)
m	mass (g)
N	number of battery cells (-)
Nu	Nusselt number (-)
P	pressure (kPa)
$\dot{q}$	heating/cooling rate (kW)
R	universal gas constant (J/mol-K)
t	time (s)
Δt	time interval (s)
T	temperature (K)
V	ventilation velocity (m/s)
Z	pre-exponential factor (1/s)

Greeks

ε	emissivity (-)
σ	Stefan–Boltzmann constant (W/m^2-K^4)
ρ	density (kg/m^3)
μ	dynamic viscosity (Pa-s)

Superscripts

*	critical

Subscripts

a	ambient
b	hot boundary
c	convective cooling
e	electrolyte
ex	external
in	internal
$loss$	heat loss
LIB	lithium-ion battery
max	maximum
p	battery pile
r	exothermic reaction
rad	radiation
TR	thermal runaway
v	safety venting

Abbreviations

EDS	energy dispersive spectrometer
LIB	lithium-ion battery
MSC	micro short circuit
SEM	scanning electron microscopy
SOC	state of charge
SS	stainless-steel
TR	thermal runaway

CRediT authorship contribution statement

References

Archibald, E., Kennedy, R., Marr, K., Jeevarajan, J., Ezekoye, O., 2020. Characterization of Thermally Induced Runaway in Pouch Cells for Propagation. Fire Technology. https://doi.org/10.1007/s10694-020-00974-2

ASTM, 2014. Standard Test Method for Hot-Surface Ignition Temperature of Dust Layers 1. ASTM E 2021-01 Standard 09, 1–10. https://doi.org/10.1520/E2021-09R13.2

Börger, A., Mertens, J., Wenzl, H., 2019. Thermal runaway and thermal runaway propagation in batteries: What do we talk about? Journal of Energy Storage 24, 100649. https://doi.org/10.1016/j.est.2019.01.012

Bravo Diaz, L., He, X., Hu, Z., Restuccia, F., Marinescu, M., Barreras, J.V., Patel, Y., Offer, G., Rein, G., 2020. Review—Meta-Review of Fire Safety of Lithium-Ion Batteries: Industry Challenges and Research Contributions. Journal of The Electrochemical Society 167, 090559. https://doi.org/10.1149/1945-7111/aba8b9

Bugryniec, P.J., Davidson, J.N., Cumming, D.J., Brown, S.F., 2019. Pursuing safer batteries: Thermal abuse of LiFePO 4 cells. Journal of Power Sources 414, 557–568. https://doi.org/10.1016/j.jpowsour.2019.01.013

Chen, H., Buston, J.E.H., Gill, J., Howard, D., Williams, R.C.E., Rao Vendra, C.M., Shelke, A., Wen, J.X., 2020. An experimental study on thermal runaway characteristics of lithium-ion batteries with high specific energy and prediction of heat release rate. Journal of Power Sources 472, 228585. https://doi.org/10.1016/j.jpowsour.2020.228585

Chen, M., Liu, J., He, Y., Yuen, R., Wang, J., 2017. Study of the fire hazards of lithium-ion batteries at different pressures. Applied Thermal Engineering 125, 1061–1074. https://doi.org/10.1016/j.applthermaleng.2017.06.131

Chen, M., Liu, J., Ouyang, D., Wang, J., 2019a. Experimental investigation on the effect of ambient pressure on thermal runaway and fire behaviors of lithium-ion batteries. International Journal of Energy Research 43, 4898–4911. https://doi.org/10.1002/er.4666

Chen, M., Ouyang, D., Weng, J., Liu, J., Wang, J., 2019b. Environmental pressure effects on thermal runaway and fire behaviors of lithium-ion battery with different cathodes and state of charge. Process Safety and Environmental Protection 130, 250–256. https://doi.org/10.1016/j.psep.2019.08.023

Cui, Y., Liu, J., 2021. Research progress of water mist fire extinguishing technology and its application in battery fires. Process Safety and Environmental Protection 149, 559–574. https://doi.org/10.1016/j.psep.2021.03.003

Drake, S.J., Wetz, D.A., Ostanek, J.K., Miller, S.P., Heinzel, J.M., Jain, A., 2014. Measurement of anisotropic thermophysical properties of cylindrical Li-ion cells. Journal of Power Sources 252, 298–304. https://doi.org/10.1016/j.jpowsour.2013.11.107

Federa Administration Aviation, 2016. New International Civil Aviation Organization (ICAO) Regulatory Requirements for Shipping and Transporting Lithium Batteries.

Federal Aviation Administration, 2018. Events With Smoke, Fire, Extreme Heat or Explosion Involving Lithium Batteries or Unknown Battery.

Feng, X., Ren, D., He, X., Ouyang, M., 2020. Mitigating Thermal Runaway of Lithium-Ion Batteries. Joule 4, 743–770. https://doi.org/10.1016/j.joule.2020.02.010

Feng, X., Zheng, S., Ren, D., He, X., Wang, L., Cui, H., Liu, X., Jin, C., Zhang, F., Xu, C., Hsu, H., Gao, S., Chen, T., Li, Y., Wang, T., Wang, H., Li, M., Ouyang, M., 2019. Investigating the thermal runaway mechanisms of lithium-ion batteries based on thermal analysis database. Applied Energy 246, 53–64. https://doi.org/10.1016/j.apenergy.2019.04.009

Fu, Y., Lu, S., Li, K., Liu, C., Cheng, X., Zhang, H., 2015. An experimental study on burning behaviors of 18650 lithium ion batteries using a cone calorimeter. Journal of Power Sources 273, 216–222.

https://doi.org/10.1016/j.jpowsour.2014.09.039

Fu, Y., Lu, S., Shi, L., Cheng, X., Zhang, H., 2018. Ignition and combustion characteristics of lithium ion batteries under low atmospheric pressure. Energy 161, 38–45. https://doi.org/10.1016/j.energy.2018.06.129

He, X., Hu, Z., Restuccia, F., Yuan, H., Rein, G., 2021. Self-heating ignition of large ensembles of Lithium-ion batteries during storage with different states of charge and cathodes. Applied Thermal Engineering 117349. https://doi.org/https://doi.org/10.1016/j.applthermaleng.2021.117349

He, X., Restuccia, F., Zhang, Y., Hu, Z., Huang, X., Fang, J., Rein, G., 2020. Experimental Study of Self-heating Ignition of Lithium-Ion Batteries During Storage: Effect of the Number of Cells. Fire Technology 56, 2649–2669. https://doi.org/10.1007/s10694-020-01011-y

Hu, Z., He, X., Restuccia, F., Rein, G., 2021a. Anisotropic and homogeneous model of heat transfer for self-heating ignition of large ensembles of lithium-ion batteries during storage. Applied Thermal Engineering 197, 117301. https://doi.org/https://doi.org/10.1016/j.applthermaleng.2021.117301

Hu, Z., He, X., Restuccia, F., Rein, G., 2020. Numerical Study of Self-Heating Ignition of a Box of Lithium-Ion Batteries During Storage. Fire Technology. https://doi.org/10.1007/s10694-020-00998-8

Hu, Z., He, X., Restuccia, F., Yuan, H., Rein, G., 2021b. Numerical study of scale effects on self-heating ignition of lithium-ion batteries stored in boxes, shelves and racks. Applied Thermal Engineering 190, 116780. https://doi.org/10.1016/j.applthermaleng.2021.116780

Huang, P., Ping, P., Li, K., Chen, H., Wang, Q., Wen, J., Sun, J., 2016. Experimental and modeling analysis of thermal runaway propagation over the large format energy storage battery module with Li4Ti5O12 anode. Applied Energy 183, 659–673. https://doi.org/10.1016/j.apenergy.2016.08.160

Huang, P., Yao, C., Mao, B., Wang, Q., Sun, J., Bai, Z., 2020. The critical characteristics and transition process of lithium-ion battery thermal runaway. Energy 213, 119082. https://doi.org/10.1016/j.energy.2020.119082

Huang, X., Gao, J., 2021. A review of near-limit opposed fire spread. Fire Safety Journal 120, 103141. https://doi.org/10.1016/j.firesaf.2020.103141

Kennedy, R.W., Marr, K.C., Ezekoye, O.A., 2021. Gas release rates and properties from Lithium Cobalt Oxide lithium ion battery arrays. Journal of Power Sources 487, 229388. https://doi.org/10.1016/j.jpowsour.2020.229388

Lamb, J., Orendorff, C.J., Steele, L.A.M., Spangler, S.W., 2015. Failure propagation in multi-cell lithium ion batteries. Journal of Power Sources 283, 517–523. https://doi.org/10.1016/j.jpowsour.2014.10.081

Lee, C., Said, A.O., Stoliarov, S.I., 2019. Impact of State of Charge and Cell Arrangement on Thermal Runaway Propagation in Lithium Ion Battery Cell Arrays. Transportation Research Record 2673, 408–417. https://doi.org/10.1177/0361198119845654

Li, H., Duan, Q., Zhao, C., Huang, Z., Wang, Q., 2019. Experimental investigation on the thermal runaway and its propagation in the large format battery module with Li(Ni1/3Co1/3Mn1/3)O2 as cathode. Journal of Hazardous Materials 375, 241–254. https://doi.org/10.1016/j.jhazmat.2019.03.116

Liu, Q., Yi, X., Han, X., 2020. Effect of Different Arrangement on Thermal Runaway Characteristics of 18650 Lithium Ion Batteries Under the Typical Pressure in Civil Aviation Transportation. Fire Technology 56, 2509–2523. https://doi.org/10.1007/s10694-020-00984-0

Liu, X., Stoliarov, S.I., Denlinger, M., Masias, A., Snyder, K., 2015. Comprehensive calorimetry of the thermally-induced failure of a lithium ion battery. Journal of Power Sources 280, 516–525. https://doi.org/10.1016/j.jpowsour.2015.01.125

Liu, Y., Sun, P., Lin, S., Niu, H., Huang, X., 2020. Self-heating ignition of open-circuit cylindrical Li-ion battery pile: Towards fire-safe storage and transport. Journal of Energy Storage 32, 101842. https://doi.org/10.1016/j.est.2020.101842

Liu, Y., Sun, P., Niu, H., Huang, X., Rein, G., 2021. Propensity to self-heating ignition of open-circuit pouch lithium-ion battery pile on a hot boundary. Fire Safety Journal 120. https://doi.org/10.1016/j.firesaf.2020.103081

Lopez, C.F., Jeevarajan, J.A., Mukherjee, P.P., 2015. Experimental analysis of thermal runaway and propagation in lithium-ion battery modules. Journal of the Electrochemical Society 162, A1905–A1915. https://doi.org/10.1149/2.0921509jes

Mao, B., Chen, H., Jiang, L., Zhao, C., Sun, J., Wang, Q., 2020a. Refined study on lithium ion battery combustion in open space and a combustion chamber. Process Safety and Environmental Protection 139, 133–146. https://doi.org/https://doi.org/10.1016/j.psep.2020.03.037

Mao, B., Huang, P., Chen, H., Wang, Q., Sun, J., 2020b. Self-heating reaction and thermal runaway criticality of the lithium ion battery. International Journal of Heat and Mass Transfer 149, 119178. https://doi.org/10.1016/j.ijheatmasstransfer.2019.119178

Nakamura, Y., Yoshimura, N., Ito, H., Azumaya, K., Fujita, O., 2009. Flame spread over electric wire in sub-atmospheric pressure. Proceedings of the Combustion Institute 32 II, 2559–2566. https://doi.org/10.1016/j.proci.2008.06.146

Nemanick, E.J., Quinzio, M. V., Joseph, P., Yong, K., Goeppinger, A., Walker, D., 2018. Li-ion 18650 Thermal Runaway Particulate Analysis.

Offer, G., Patel, Y., Hales, A., Bravo Diaz, L., Marzook, M., 2020. Cool metric for lithium-ion batteries could spur progress. Nature 582, 485–487. https://doi.org/10.1038/d41586-020-01813-8

Ping, P., Kong, D., Zhang, J., Wen, R., Wen, J., 2018. Characterization of behaviour and hazards of fire and deflagration for high-energy Li-ion cells by over-heating. Journal of Power Sources 398, 55–66. https://doi.org/10.1016/j.jpowsour.2018.07.044

Qin, P., Sun, J., Wang, Q., 2021. A new method to explore thermal and venting behavior of lithium-ion battery thermal runaway. Journal of Power Sources 486, 229357. https://doi.org/10.1016/j.jpowsour.2020.229357

Said, A.O., Lee, C., Stoliarov, S.I., 2020. Experimental investigation of cascading failure in 18650 lithium ion cell arrays: Impact of cathode chemistry. Journal of Power Sources 446, 227347. https://doi.org/10.1016/j.jpowsour.2019.227347

Sun, J., Mao, B., Wang, Q., 2021. Progress on the research of fire behavior and fire protection of lithium ion battery. Fire Safety Journal 120, 103119. https://doi.org/10.1016/j.firesaf.2020.103119

Sun, P., Bisschop, R., Niu, H., Huang, X., 2020. A Review of Battery Fires in Electric Vehicles. Fire Technology 56, 1361–1410. https://doi.org/10.1007/s10694-019-00944-3

Sun, P., Zhang, X., Ding, C., Huang, X., 2021. Effect of reduced pressure on burning dynamics of fire whirls. Fire Safety Journal 125, 103419. https://doi.org/10.1016/j.firesaf.2021.103419

Torres-Castro, L., Kurzawski, A., Hewson, J., Lamb, J., 2020. Passive Mitigation of Cascading Propagation in Multi-Cell Lithium Ion Batteries. Journal of The Electrochemical Society 167, 090515. https://doi.org/10.1149/1945-7111/ab84fa

United Nations, 2019. Recommendations on the Transport of Dangerous Goods - Model Regulations (Twenty-First Revised edition).

Wang, H., Du, Z., Liu, L., Zhang, Z., Hao, J., Wang, Q., Wang, S., 2020a. Study on the Thermal Runaway and Its Propagation of Lithium-Ion Batteries Under Low Pressure. Fire Technology 56, 2427–2440. https://doi.org/10.1007/s10694-020-00963-5

Wang, H., Du, Z., Rui, X., Wang, S., Jin, C., He, L., Zhang, F., Wang, Q., Feng, X., 2020b. A comparative analysis on thermal runaway behavior of Li (NixCoyMnz) O2 battery with different nickel contents at cell and module level. Journal of Hazardous Materials 393, 122361.

https://doi.org/10.1016/j.jhazmat.2020.122361

Wang, Q., Mao, B., Stoliarov, S.I., Sun, J., 2019. A review of lithium ion battery failure mechanisms and fire prevention strategies. Progress in Energy and Combustion Science 73, 95–131. https://doi.org/10.1016/j.pecs.2019.03.002

Wang, Y.W., Huang, C.Y., 2020. Thermal explosion energy evaluated by thermokinetic analysis for series- and parallel-circuit NMC lithium battery modules. Process Safety and Environmental Protection 142, 295–307. https://doi.org/10.1016/j.psep.2020.06.009

Wang, Z., Mao, N., Jiang, F., 2020. Study on the effect of spacing on thermal runaway propagation for lithium-ion batteries. Journal of Thermal Analysis and Calorimetry 140, 2849–2863. https://doi.org/10.1007/s10973-019-09026-6

Weng, J., Ouyang, D., Liu, Y., Chen, M., Li, Y., Huang, X., Wang, J., 2021. Alleviation on battery thermal runaway propagation: Effects of oxygen level and dilution gas. Journal of Power Sources 509, 230340. https://doi.org/10.1016/j.jpowsour.2021.230340

Weng, J., Ouyang, D., Yang, X., Chen, M., Zhang, G., Wang, J., 2019. Alleviation of thermal runaway propagation in thermal management modules using aerogel felt coupled with flame-retarded phase change material. Energy Conversion and Management 200, 112071. https://doi.org/10.1016/j.enconman.2019.112071

Xie, S., Ren, L., Gong, Y., Li, M., Chen, X., 2020a. Effect of Charging/Discharging Rate on the Thermal Runaway Characteristics of Lithium-Ion Batteries in Low Pressure. Journal of The Electrochemical Society 167, 140503. https://doi.org/10.1149/1945-7111/abbfd8

Xie, S., Ren, L., Yang, X., Wang, H., Sun, Q., Chen, X., He, Y., 2020b. Influence of cycling aging and ambient pressure on the thermal safety features of lithium-ion battery. Journal of Power Sources 448, 227425. https://doi.org/10.1016/j.jpowsour.2019.227425

Xie, S., Sun, J., Chen, X., He, Y., 2020c. Thermal runaway behavior of lithium-ion batteries in different charging states under low pressure. International Journal of Energy Research 1–11. https://doi.org/10.1002/er.6200

Yuan, L., Dubaniewicz, T., Zlochower, I., Thomas, R., Rayyan, N., 2020. Experimental study on thermal runaway and vented gases of lithium-ion cells. Process Safety and Environmental Protection 144, 186–192. https://doi.org/10.1016/j.psep.2020.07.028

Yuan, S., Chang, C., Yan, S., Zhou, P., Qian, X., Yuan, M., Liu, K., 2021. A review of fire-extinguishing agent on suppressing lithium-ion batteries fire. Journal of Energy Chemistry. https://doi.org/10.1016/j.jechem.2021.03.031

Zhou, Z., Zhou, X., Peng, Y., Li, L., Cao, J., Yang, L., Cao, B., 2021. Quantitative study on the thermal failure features of lithium iron phosphate batteries under varied heating powers. Applied Thermal Engineering 185, 116346. https://doi.org/10.1016/j.applthermaleng.2020.116346